IFAC-PapersOnLine, Volume 53, Issue 3, 2020, pp. 66-71
DOI: 10.1016/j.ifacol.2020.11.011

A miniaturised active thermography system for in-situ inspections

Weixiang Du [a], Haochen Liu [a], Adisorn Sirikham [a], Sri Addepalli [a], Yifan Zhao [a*]

[a] Through-Life Engineering Services Institute, Cranfield University, Cranfield, MK43 0AL, United Kingdom
[*]Corresponding author: Tel.: +44 (0)1234 754729, E-mail yifan.zhao@cranfield.ac.uk

Abstract: With the increase of the functionalisation, integration and complexity of industrial components and systems, deploying Non-Destructive Testing (NDT) devices for 'in-situ' inspection has become a major challenge for high-value assets. Due to the mismatching of size and volume between the existing inspection unit and the targeted complex object, inaccessibility and inapplicability have limited the applicability of NDT techniques. To address this challenge, this paper introduces a novel miniaturised active thermography system based on a commercial thermal imaging sensor featured with small size and low cost. Combining with different excitation sources, its detection performance on different types of defect of carbon fibre reinforced polymer (CFRP) is investigated and compared with an existing system. The results show that the proposed system can work with laser and flash effectively for degradation assessment although the detectability is compromised. Such a technique will play a unique role in the in-situ inspection where the space to deploy the device is limited.

Keywords: Pulsed thermography; Laser thermography; Degradation assessment; Signal analysis

1. INTRODUCTION

In the field of aerospace (Conshohocken, 2007), transportation (Bien, Hoła, & Sadowski, 2013) and energy industries (Yang, Zhang, Zhang, & Ai, 2013), the damage of key components endangers the overall safety and integrity of the structure. Non-Destructive Testing (NDT) is a well-known and promising technique for accurately detecting the defects or material non-uniformity without damaging and undermining the performance of the system. However, with the increasing integration levels and complexity of industrial systems, the size and volume of NDT equipment become a bottleneck to improve the accessibility and applicability of the inspection. At the same time, the serviceability of the components or systems to be inspected has now become challenging, particularly in determining their maintenance requirements as disassembly and inspection is very expensive. Therefore, it is essential to develop lightweight and miniaturised NDT system for the degradation evaluation of components or systems with limited space for inspection.

Visual and optical testing has the characteristics of being intuitive, non-contact and fast speed, but they are limited to detecting surface defects (Kroworz & Katunin, 2018). Penetration testing is only suitable for the surface inspection of non-porous materials (Phong & Yan, 2014). Magnetic particle inspection is only suitable for ferromagnetic materials inspection, and the lift force of the yoke and defect detection rate will go down when the volume of the device decrease (Harding & Hugo, 2013). Eddy current detection has high detection efficiency, but it is only capable of inspecting conductive materials (García-Martín, Gómez-Gil, & Vázquez-Sánchez, 2011). Radiographic testing can achieve accurate inspection for internal defects, but its application is limited by the high-cost and safety issues. Ultrasonic inspection is another widely used inspection method, which can perform accurate measurements with good penetration depth. However, the coupling agents and the blind regions on the surface limit its application for complex-shaped workpieces with a small thickness (Du, Zhao, Roy, Addepalli, & Tinsley, 2018). Responding to the demand for in-situ inspection, the above disadvantages drag down the progress and applications of corresponding NDT techniques in specific scenarios.

Infrared (IR) thermography is one of the most popular NDT methods for inspection defects. In this approach, an external energy source heats a sample in a non-contact manner and generates a temperature contrast at material discontinuities. As a powerful NDT technology, infrared thermography can provide rapid, non-contact, and robust non-invasive detection with real-time monitoring. It is widely used in fault diagnosis, quality control, and condition monitoring. The thermography test can be divided into two modes: passive and active thermography (Kirimtat & Krejcar, 2018). The difference lies in whether the heat flow in the targeted object is generated by external excitation energy or is inherent to the system itself. For active thermography, the excitation source can be divided into three categories: optical, mechanical and induction excitation. Both flash and laser belong to optical excitation, ultrasonic belongs to mechanical excitation (Zhang et al., 2019), and eddy current is a typical representative of induction excitation (Gao, Bai, Woo, Tian, & Cheng, 2014). The flash has the advantages of covering large excitation area with fast speed, but due to the factors such as irradiation distance and energy attenuation, the working distance should not be too far. Compared to flash, the laser has advantages in energy density, intensity, accuracy, and adjustability (Pei, Liu, Qiu, Liu, & Chen, 2019). It is an ideal light source for remote detection of

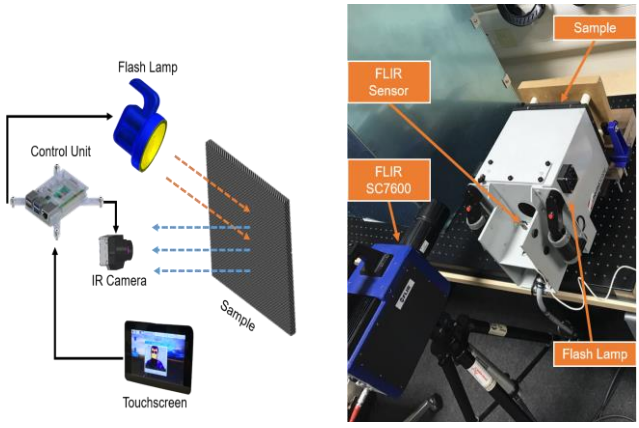

(a) MAT system (excitation source: flash)

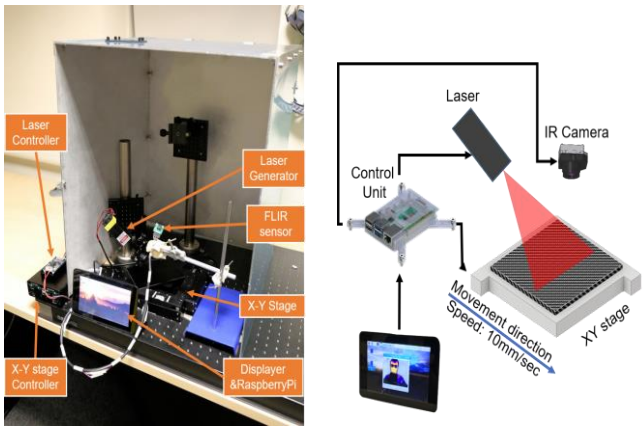

(b) MAT system (excitation source: laser)

Fig. 1. The proposed miniaturised Active Thermography (MAT) system.

Table 1. Specification of the tested two cameras

Specification	FLIR SC7600	FLIR Lepton
waveband	Mid-Wave	Long-Wave
Spectral ranges	1.5-5.1μm	8-14 μm
Pixel Resolution	640x512	160x120
Pixel Pitch	15μm	12 μm
NETD	<20mK	<50mK
Full Frame Rate	100HZ	8.7HZ
Accuracy	±1°C or ±1%	±5°C or ±5%
Size (L×W×H)	403×130×168 mm	12.7×11.5×7.14 mm
Weight	4950 g	0.91 g

delamination or cracking defects in composites. Comparing with eddy current induction, the attenuation of the laser beam is very low, and achieves long-distance heating capacity, its flexible directionality supports its application in a narrow space scenario. At the same time, for the detection of sub-surface defects of composite materials, a high-energy and easy-to-control laser spot provides better heating uniformity and a higher temperature signal-to-noise ratio, which also provides a solid foundation for accurate quantitative assessment of defects. In addition, due to the high-quality quantum detectors used in infrared cameras, especially the indium antimonide and mercury cadmium telluride versions, the price of infrared cameras has become another factor restricting their deployment for in-situ inspections. Considering large scale of tasks in in-situ inspection, low-cost and small-size infrared cameras are attractive for the stakeholders and inspection environment, but they usually compromise in spatial resolution, noise resistance, thermal sensitivity and sampling rate. It is meaningful and economical to develop a low-cost and miniaturised infrared thermography system with satisfactory sensing capability, especially for rapid screening of defects for large components.

At present, the existing miniaturised infrared cameras are mostly used in passive IR detection, while very few studies investigated its application in active thermography inspection. This paper reports a novel miniaturised active thermography (MAT) system which consists of a commercial IR sensor and flash and laser excitation sources. Through experiments, the defect detectability of this system is evaluated qualitatively and quantitatively. The inspected results and performance are verified by a high-resolution thermography system.

2. MAT SYSTEM DESIGN AND THERMAL

2.1 MAT system setup

The proposed MAT system consists of a miniaturised commercial infrared sensor, FLIR Lepton (FLIR, n.d.), and the external excitation source, which are integrated with a Raspberry Pi 3B+ with a 7-inch touch screen (as seen in Fig.1). Comparing with other IR cameras, such as FLIR SC7600 (Sirikham, Zhao, Nezhad, Du, & Roy, 2019), FLIR A655sc (Du, Addepalli, & Zhao, 2019)for active thermography, Lepton sensor is relatively small with a size similar to a 5 UK pence coin. Even if it is embedded into an external board, the size is just similar to a UK 10 pence, as shown in Fig. 2. Table 1 shows the comparison of the specification of FLIR SC7600 and FLIR Lepton, which will be tested in this paper. SC7600 has 16 time higher spatial-resolution and more than 5000 times heavier weight than Lepton. The cost of SC7600 is much higher than the Lepton.

The MAT system carries two different sets of excitation sources: optical flash and laser. The combination of excitation sources establishes flexibility to detect a variety of defects.

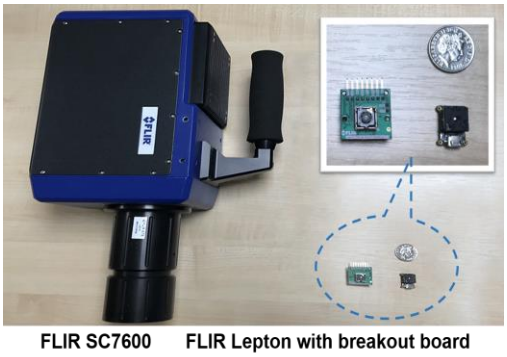

Fig. 2. Comparison of the FLIR lepton with SC7600 for active thermography

The pulsed MAT system is powered by capacitor bank controlled twin xenon flash lamps assembled inside a box with internal reflectors with a nominal flash power output of 2KJ (see Fig. 1(a)). The flash energy can be adjusted to pulse heat different samples in adjustable working distance between 200mm to 300mm. The laser MAT system (see Fig. 1(b)) employs a low-cost semiconductor laser generator with 450nm wavelength, and the laser head dimension is 86 ×33 ×33 mm. This small size, directionality and figurability of laser allows the proposed MAT system working under narrow space. The 15W laser beam is shaped to a line using an optical shaping lens.

Dedicated software is developed and integrated with the Raspberry Pi to capture, store and process the data. The raw thermal images and inspection results can be visualised by a mini touch screen.

2.2 Data processing

Based on the Fourier heat transfer law, the surface temperature due to a defect at depth L for a plate is given by (Zhao, Addepalli, Sirikham, & Roy, 2018).

$$T(t) = \frac{Q}{\sqrt{\pi\rho ckt}}\left[1 + 2\sum_{n=1}^{\infty} exp\left(-\frac{n^2L^2}{\alpha t}\right)\right] \quad (1)$$

where $T(t)$ is the temperature variation of the surface at time t, Q is the pulse energy, ρ,c k are the material density, the specific heat capacity and the thermal conductivity respectively. The α is the thermal diffusivity of the material.

In the pulsed MAT system, the thermal images are processed using the Logarithmic Second-Derivative method (LSD) (Shepard, 2003) and the New Least-squares Fitting (NLSF) method (Sirikham, Zhao, & Mehnen, 2017). LSD is a classic approach of depth estimation for pulsed thermography where the temperature decay curve is converted into the logarithmic domain, and then the curve is fitted with a polynomial model to reduce temporal noise and save storage space. The fitting method is called Thermal Signal Reconstruction (TSR). The peak of the second derivative of the TSR fitting is often used to estimate the depth of the defect. The polynomial model is written as：

$$\ln(\mathrm{T(t)}) = \sum_{n=0}^{N} a_n (ln(t))^n \quad (2)$$

where N is the order of the polynomial function, a_n are polynomial coefficients to be estimated. The first derivative of TSR can be directly computed by

$$\frac{\mathrm{d}\ln(\mathrm{T(t)})}{dln(t)} = \sum_{n=1}^{N} a_n \cdot n \cdot (ln(t))^{n-1} \quad (3)$$

And the second derivative of TSR can be computed by

$$\frac{\mathrm{d}^2\ln(\mathrm{T(t)})}{\mathrm{d}^2 ln(t)} = \sum_{n=2}^{N} a_n \cdot n \cdot (n-1) \cdot (ln(t))^{n-2} \quad (4)$$

The Least-squares Fitting (LSF) method (Sun, 2003)uses a curve-fitting approach based on a 1-D heat transfer model to fit the temperature decay curve to identify the defect depth. This method has good resistance to noise, but it assumes a thermal wave reflection coefficient (R) of 1, which is not valid in most real situations. The NLSF method estimates the value of R directly from the observation data and has a higher accuracy of defect depth estimation. The analytical model of NLSF is written as follows:

$$\tilde{T}(t, A, W, R, t_s, s) = \frac{A}{\sqrt{t + t_s}}\left[1 + 2\sum_{n=1}^{M} R^n exp\left(-\frac{n^2 W}{t + t_s}\right)\right] - s(t + t_s) \quad (5)$$

where A=$\frac{Q}{\sqrt{\pi\rho ck}}$, W=$\frac{L^2}{\alpha}$, L is the defect depth or the thickness of the sample, α is the thermal diffusivity, R is the thermal wave reflection coefficient, t is sampling duration, t_s is the starting time of sampling, s is the slope, and M is a large iteration number. There are five parameters to be estimated including A, W, R, t_s, and s. A nonlinear least-squares solver in MATLAB (*lsqnonlin*) is applied to solve this five-parameter optimization problem.

In the laser MAT system, the Savitzky-Golay smoothing filter was used to increase the SNR of severely corrupted IR images from Lepton. This is achieved by fitting successive time frames (or within a time window) with a pre-defined degree polynomial. As in the case of scattered signals, when the data points are equally spaced, an analytical solution can be derived in the form of a single set of convolution coefficients. The equation is written as:

$$x_{j,smooth} = \bar{x}_j = \frac{1}{N}\sum_{i=-m}^{i=m} C_i Y_{j+i} \quad (6)$$

where C_i is the smoothing factor. For the moving average, each C_i is equal to one and N is the number of convolution integers. j represents the running index. Y_{j+i} is the observed value of data points.

The 1st and 2nd derivatives of the filtered IR images can reduce noise and enhance the true defect. It should be noted that, in this study, the relative position between the laser and IR camera is fixed while the laser line is always on. In raw IR images, the intensity of the laser line is so high that the contrast of defect is very low and becomes almost invisible. The 1st or 2nd derivative between two adjacent frames will completely remove the laser line and preserve the change between these two images, by which means the contract of defect is significantly enhanced.

2.3 Experiments

2.3.1 Samples

This paper employs three CFRP samples with different kinds of defects, marked as Sample 1, Sample 2 and Sample 3. All samples were made by unidirectional Toray 800 carbon fibres pre-impregnated with Hexcel M21 epoxy resin. Sample 1 has a dimension of 155 × 155 × 8 mm which contains 16 artificial flat-bottomed defects. The specification of Sample 1 can be seen in Fig. 3, where Point 1-16 indicate different defects and Point 0 is sampled from the sound region (reference region). The defects are arranged in 4 by a 4 array layout, and the centre distance between each hole is 31mm. As illustrated in Fig. 3(b),

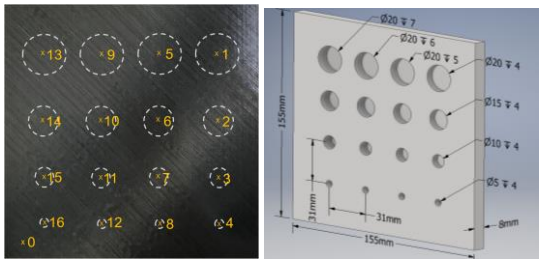

(a) Front side (b) Back side (3D view)

Fig. 3. Illustration of Sample 1. (a) Dash circle indicates the dimensions and locations of defects on the backside. Point 1-16 mark different defect and Point 0 is sampled from a sound region (reference region) (b) Design dimensions of defects on the backside.

the holes were drilled with four groups of diameters (5, 10, 15, and 20 mm) and four groups of thicknesses (7, 6, 5, and 4 mm), representing defect depths at 1, 2, 3, and 4 mm, from the surface. The defects in each row have the same diameter and different depth, while the holes in each column have different diameter but the same depth. The design of this sample helps to qualitatively and quantitatively analyse the detection performance of the pulsed MAT system comparing to the high-resolution equipment.

The dimension of Sample 2 and Sample 3, made by CFRP as well, are 150 × 120 × 5 mm, where impact damage is presented. Sample 2 contains the 42 mm length impact based compound defect, and features both crack and delamination. Sample 3 has a 22 mm "Zigzag" shaped crack with the fibres and the matrix of the CFRP surface. The inspection and measurement of these complex defects and damage are crucial to the life-assessment and maintenance of a composite structure.

2.3.2 Experiments design

Two experiments were implemented for these three samples. For the comparison purpose, the first experiment was conducted on Sample 1 using MAT and SC7600 under the same experiment condition. A flash excitation source was used to provide a homogenous and large area heating for back-drilled hole defects of Sample 1. Comparing to laser, a quick pulse is a suitable excitation for detecting the wall-thinning damage.

The working distance from the two cameras to the sample surface is 250 mm. The flash energy applied to the sample was 2kJ. The framerate of Lepton and SC7600 were set at 8.7 Hz and 10 Hz, respectively. The whole inspection duration is 70 s, with 609 and 700 frames being captured by two cameras, respectively.

Experiment 2 was conducted on Sample 2 and 3 where a laser excitation source and Lepton sensor were used. The line laser beam is projected on the sample surface with a 45° angle. The laser energy is 15W. The framerate of the Lepton sensor was set as the same as Experiment 1. The camera vertically works at 100mm distance away from the sample surface. An automatic XY stage facilitated the movement of the sample at a speed of 10mm/sec. The samples were fixed on the XY stage, keep the laser and IR lens still, and let the XY stage move at a constant speed.

3. RESULT AND DISCUSSION

3.1 Result of Experiment 1

To illustrate the detectability of defects with different depths, the maximal temperature contrast appears at different times, Fig. 4(a)-(c) show the 35th, 144th and 155th thermal images from SC7600 and Fig. 4(a)-(c) show the 49th, 145th and 186th frames from the proposed MAT system. Due to the diversity of the dimension and depth, defects can be seen from different temporal images. The defects with shallow surface depth appear earlier. In addition, relatively sharp edges can be observed on the biggest defects, while the results of smaller ones have blurred edges. It can be observed that not all defects can be detected. SC7600 can detect 10 defects representing Point 1, 2, 3, 4, 5, 6, 7, 9, 10,11 while Lepton can inspect 6 defects representing Point 1, 2, 3, 4, 5, 6, as shown in Table 2.

Fig. 5 plots the temperature-time decay curves in the logarithmic domain from SC7600 and MAT. Fig. 5(a) and (c) show the curves of defects with the same depth but different size, as well as the reference. Fig. 5(b) and (d) show the curves of defects with the same size but different depth. It can be seen from the comparison that SC7600 has clearly better signal quality than the Lepton sensor. However, the MAT system can effectively capture the difference of decay curve among the

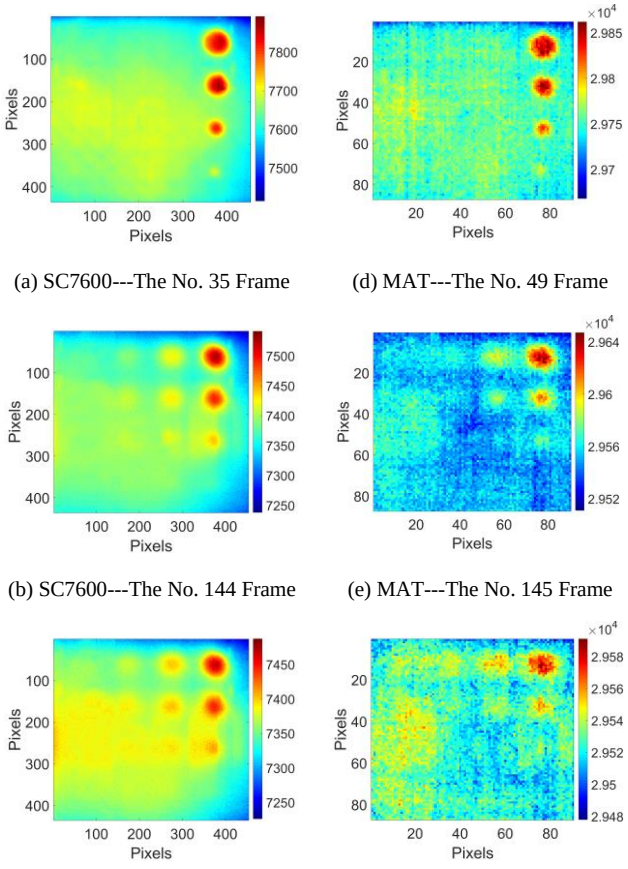

(a) SC7600---The No. 35 Frame (d) MAT---The No. 49 Frame

(b) SC7600---The No. 144 Frame (e) MAT---The No. 145 Frame

(c) SC7600---The No. 175 Frame (f) MAT---The No. 186 Frame

Fig. 4. The raw thermal images at different times for Sample 1.

Table 2. Comparing the inspection result of Sample 1 defects regions using FLIR SC7600 and MAT

	FLIR SC7600	MAT
The numbers of the defect holes can be detected	1,2,3,4,5,6, 7,9,10,11	1,2,3,4,5,6
The Min defect ϕ can be detected	Φ5	Φ5
The Max defect Depth can be detected	3mm	2mm

selected defects and the reference, which clearly suggests the effectiveness of the proposed MAT system.

Table 3 shows the estimated defect depths of the selected points using the LSD and NLSF methods using two systems. For the same defect, SC7600 measures the depth more accurately (error up to 11%) than MAT (error up to 25%). Comparing the results of the same pixel position, the accuracy of the NLSF method is better than the LSD method. Although, not surprisingly, the high-resolution camera is superior to the MAT system in the overall detection accuracy, the results of the MAT system are acceptable and sufficient to detect certain defects. Fig. 6 plots a capability polygon map of two cameras using LSD and NLSF for Sample 1. It can be clearly observed that although SC7000 with flash excitation performs better than pulsed MAT for both approaches of depth measurement, the performance of NLSF based on MAT is similar to that of LSD with SC7000. This observation suggests that NLSF is a more appropriate approach to analyse the data from MAT due to its better performance to tackle high-level noise (Sirikham et al., 2017).

3.2 Result of Experiment 2

As shown in the 89th frame of the raw thermal images of Sample 2 (see the left graph of Fig. 7), the compound defects are presented with high contrast. However, there is a laser beam beside the defect, which interferes with the result. After applying the Savitzky-Golay smoothing filter, the first and second derivative of the filtered IR images (see the middle and right graphs) presents the defects with high-contrast contours and details of the defects texture, where the laser beam has removed from the image. For Sample 3, the 93rd raw thermal image is presented in Fi. 7, where the defect overlaps with the laser beam and leads to the unclear results. The first and second derivatives also solve this problem. In addition, the first and second derivatives can well separate the layered and crack defects from the thermal imaging, particularly for Sample 2.

4. CONCLUSION

Aiming to improve the applicability and accessibility of active thermography and simultaneously reduce the cost of the inspection equipment, a novel MAT system was proposed to qualitatively and quantitatively detect defects in industrial composite materials. Integrated with Raspberry Pi and multiple exciting sources, the proposed MAT system is able to detect multiple kinds of defects in composite material.

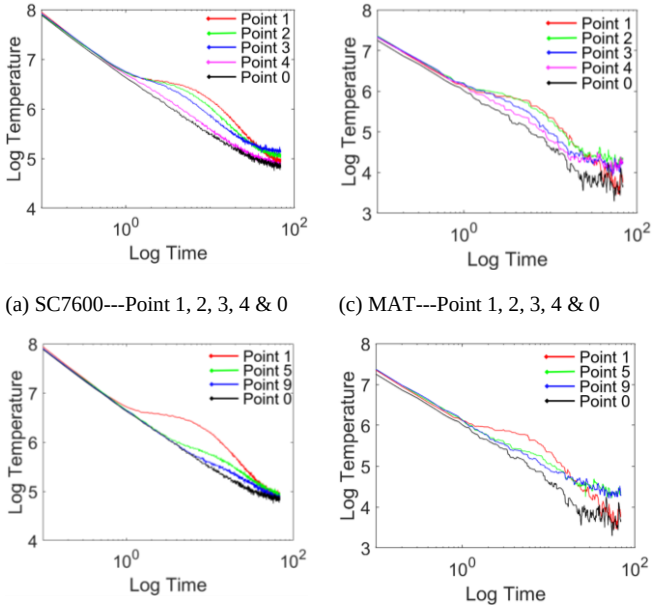

(a) SC7600---Point 1, 2, 3, 4 & 0

(c) MAT---Point 1, 2, 3, 4 & 0

(b) SC7600---Point 1, 5, 9 & 0

(d) MAT---Point 1, 5, 9 & 0

Fig. 5. Comparison of the temperature-time decay profiles in the logarithmic domain of the selected defects

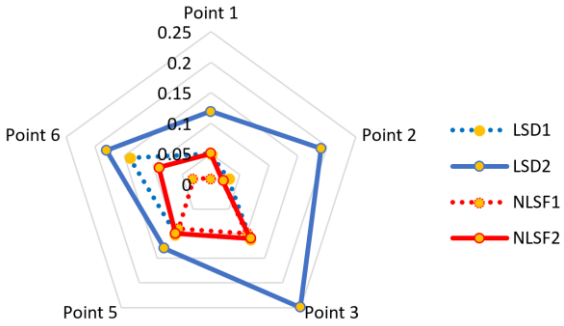

Fig. 6 The error range of FLIR SC7600 and MAT system using LSD and NLSF methods, where LSD1 and NLSF1 come from FLIR SC7600 (dash line), and LSD2 and NLSF2 come from MAT(solid line).

Compared to an existing system with a high-end infrared sensor, the proposed system has a prominent price advantage and miniaturised volume. Its mini and flexible body will better adapt to complex and varied application scenarios in the industrial in-situ inspection. Additionally, the addition of different excitation sources also allows inspecting different types of near and sub-surface defects.

It can be inferred from the experimental results that the MAT system is competent for CFRP defect inspection. All defects are presented visually with proper contrast. The experimental results show that MAT has an acceptable level of detecting near and sub-surface defects occurring in CFRP laminates. In the experiment of the flat-bottom hole sample, the maximum detectable depth is 2mm, and the minimum diameter is 5mm. The laser excitation for the MAT system achieved good detection results for cracks and delamination defects, especially after the first and second derivative of TSR process,

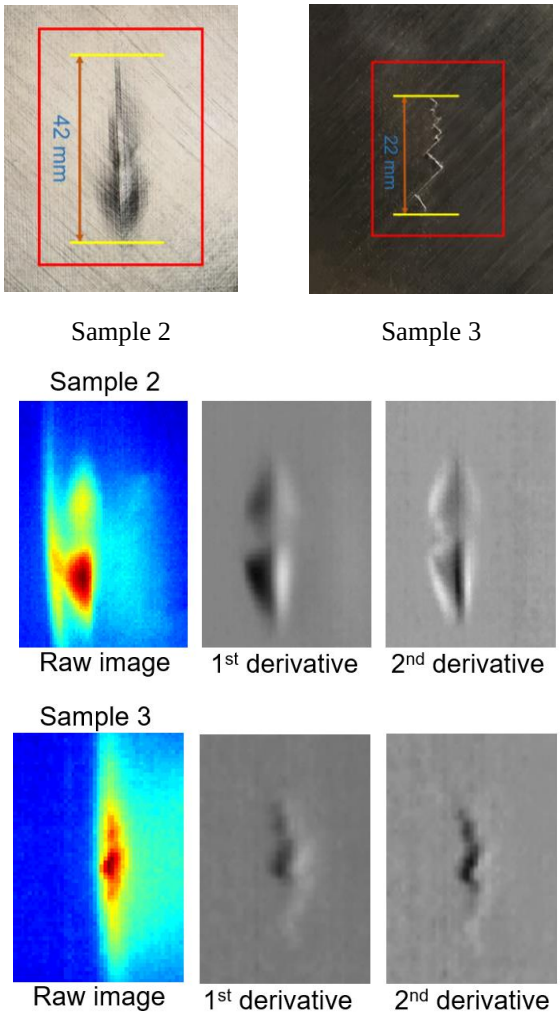

Fig. 7 Laser MAT system defect inspection for Sample 2 and 3, where the snapshot of sample 2 is from 89th frame, and the snapshot of Sample 3 is from 93rd frame

the laser beam and other noise has been removed, the result displays well.

REFERENCE

Bien, J., Hoła, J., & Sadowski, Ł. (2013). Modern NDT Techniques in Diagnostics of Transport Infrastructure Concrete Structures. *NDT in Canada 2013 Conference in Conjuction with International Workshop on Smart Materials, Structures, SHM & NDT for the Energy Industry, Alberta, Canada*.

Conshohocken, W. (2007). Standard Practice for Infrared Flash Thermography of Composite Panels and Repair Patches Used in Aerospace Applications 1, *i*(July), 1–6.

Du, W., Addepalli, S., & Zhao, Y. (2019). The Spatial Resolution Enhancement for a Thermogram Enabled by Controlled Sub-pixel Movements. *IEEE Transactions on Instrumentation and Measurement*, 1–1.

Du, W., Zhao, Y., Roy, R., Addepalli, S., & Tinsley, L. (2018). A review of miniaturised Non-Destructive Testing technologies for in-situ inspections. *Procedia Manufacturing*, *16*, 16–23.

FLIR. (n.d.). LEPTON 3. Retrieved from http://www.flir.co.uk/cores/lepton/

Gao, B., Bai, L., Woo, W. L., Tian, G. Y., & Cheng, Y. (2014). Automatic Defect Identification of Eddy Current Pulsed Thermography Using Single Channel Blind Source Separation. *IEEE Transactions on Instrumentation and Measurement*, *63*(4), 913–922.

García-Martín, J., Gómez-Gil, J., & Vázquez-Sánchez, E. (2011). Non-destructive techniques based on eddy current testing. *Sensors*, *11*(3), 2525–2565.

Harding, C. A., & Hugo, G. R. (2013). Review of Literature on Probability of Detection for Magnetic Particle Nondestructive Testing, 1–50.

Kirimtat, A., & Krejcar, O. (2018). A review of infrared thermography for the investigation of building envelopes: Advances and prospects. *Energy and Buildings*, *176*, 390–406.

Kroworz, A., & Katunin, A. (2018). Non-destructive testing of structures using optical and other methods: A review. *SDHM Structural Durability and Health Monitoring*, *12*(1), 1–17.

Pei, C., Liu, H., Qiu, J., Liu, T., & Chen, Z. (2019). Progress on the ultrasonic testing and laser thermography techniques for NDT of tokamak plasma-facing components. *Theoretical and Applied Mechanics Letters*, *9*(3), 180–187.

Phong, C. T., & Yan, W. Q. (2014). An overview of penetration testing. *International Journal of Digital Crime and Forensics*, *6*(4), 50–74.

Shepard, S. M. (2003). Reconstruction and enhancement of active thermographic image sequences. *Optical Engineering*, *42*(5), 1337.

Sirikham, A., Zhao, Y., & Mehnen, J. (2017). Determination of thermal wave reflection coefficient to better estimate defect depth using pulsed thermography. *Infrared Physics & Technology*, *86*, 1–10.

Sirikham, A., Zhao, Y., Nezhad, H. Y., Du, W., & Roy, R. (2019). Estimation of Damage Thickness in Fiber-Reinforced Composites using Pulsed Thermography. *IEEE Transactions on Industrial Informatics*, *15*(1), 445–453.

Sun, J. (2003). Method for determining defect depth using thermal imaging, *2*(12).

Yang, B., Zhang, L., Zhang, W., & Ai, Y. (2013). Non-destructive testing of wind turbine blades using an infrared thermography: A review. *ICMREE 2013 - Proceedings: 2013 International Conference on Materials for Renewable Energy and Environment*, *1*, 407–410.

Zhang, X., He, Y., Chady, T., Tian, G., Gao, J., Wang, H., & Chen, S. (2019). CFRP Impact Damage Inspection Based on Manifold Learning Using Ultrasonic Induced Thermography. *IEEE Transactions on Industrial Informatics*, *15*(5), 2648–2659.

Zhao, Y., Addepalli, S., Sirikham, A., & Roy, R. (2018). A confidence map based damage assessment approach using pulsed thermographic inspection. *NDT & E International*, *93*(September 2017), 86–97.

A miniaturised active thermography system for in-situ inspections

Du, Weixiang

2020-12-18

Du W, Liu H, Sirikham A, et al., (2020) A miniaturised active thermography system for in-situ inspections. IFAC-PapersOnLine, Volume 53, Issue 3, 2020, pp. 66-71
https://doi.org/10.1016/j.ifacol.2020.11.011